Lateral guidance and control for a fixed-wing aircraft.

Martínez-Ramírez Marco A.*, Rodríguez-Cortés H.* and Corona-Sánchez José J.†
*Centro de Investigación y de Estudios Avanzados del Instituto Politécnico Nacional,
Sección de Mecatrónica, Departamento de Ingeniería Eléctrica,
Av. Instituto Politénico Nacional, San Pedro Zacatenco, 07360, México, D.F., México
†UiT, The Arctic University of Norway,
Department of electrical engineering (IET),
Lodve Langesgate 2, 8514 Narvik, Noruega

Abstract

This paper presents a solution to the guidance problem, taking into account the geometric properties of the aircraft kinematics. The control design considers a longitudinal dynamics controller that golds the flight path angle and aerodynamic speed at some constant references. The proposed guidance algorithm follows the inner-outer control loops approach. The inner control loop is based on a second-order sliding mode technique, while the outer control loop is designed following a nonlinear geometric control method. Numerical co-simulations employing Matlab-Simulink and the flight simulator X-Plane are presented to verify the performance of the guidance algorithm.

1 Introduction

Unmanned aerial vehicles (UAV) applications such as precision agriculture, meteorological monitoring, and ground vehicle tracking require a navigation, flight guidance, and control (NGC) system to track Cartesian plane trajectories. Since fixed-wing aircraft have advantages over rotary-wing vehicles, such as endurance and speed, they can cover a wide surface faster than their counterpart rotary-wing configuration. Thus, fixed-wing aircraft are more suitable for such applications. In fixed-wing aircraft, trajectory tracking in the Crtesian plane requires commanding the lateral-directional dynamic.

The aircraft control literature identifies two approaches to solving fixed-wing aircraft guidance and control problems. In the first approach, the problem is solved with two control loops. An outer loop determines the reference for bank angle based on the desired yaw angle and lateral distance to the desired path. An inner control loop defines the behavior of the control surfaces to follow the references from the outer control loop [1], [2], [3], [4]. In the second approach, a single control loop defines the references and actions of the control surfaces [5]. An intermediate approach integrates guidance and control schemes, as reported in [6].

Reference [2] proposes a conventional proportional and derivative (PD) lateral controller with some nonlinear improvements that enhance UAV tracking performance for different flight conditions, especially recovery from significant cross-track errors. The response of this controller is comparable with the results reported in [3], which proposed a control logic that approximates a proportional-derivative (PD) controller when following a straight-line path and contains anticipatory control terms to enable tracking curved paths. The work in [4] proposes a proportional-integral-derivative (PID) guidance law designed into two parts, a linear time-invariant (LTI) component in the forward path and a time-varying gain in the feedback path; the stability analysis is performed under the circle criterion. The stability properties of the proposed guidance law are less conservative than proportional navigation (PN) [7], proportional-derivative navigation (PDN) [8], and proportional-integral navigation (PIN) [9] guidance laws. In [10], a high-precision, globally stable 3D path tracking algorithm is proposed. The feasibility and performance are evaluated through flight tests. The guidance algorithm combines the smooth representation of the reference trajectory with flatness-based feedforward controls and a nonlinear feedback scheme based on dynamic inversion. Reference [11] develops a guidance law based on "good helmsman" behavior. The integration of the guidance law and the aircraft dynamics, maintaining closed-loop stability, is ensured. An observer to estimate wind data to orient path geometry about the target completes the algorithm. The performance of the algorithm is evaluated using a high-fidelity simulation.

A common characteristic in the works [2], [3] and [4] relies on the geometry of the desired and current aircraft positions and the decomposition of the aircraft lift force when performing a bank turn. A different approach was initiated in [12], where the aircraft kinematics structure is considered to design the guidance algorithm. In [13] the similarities between the aircraft kinematic model and the unicycle mobile robot are reported, pointing out that the only difference is that the aircraft kinematic model

*Email address(es): {marcoa.martinez,hrodriguez}@cinvestav.mx
†Email address(es): jose.j.sanchez@uit.no

cannot change the sign of the aircraft speed, imposing a decisive condition for control design. A control Lyapunov function (CLF) approach is followed to design a guidance algorithm. All feasible constrained inputs are characterized from a CLF for the input constrained case. The feasible set provides the control input.

This paper aims to presents a solution to an aircraft guidance problem using the inner-outer control loops approach. The super-twisting algorithm approach tailors the inner control loop, and the outer control loop is based on nonlinear control methods considering the geometric properties of the aircraft kinematics. In order to verify the performance of the guidance algorithm, a numerical co-simulation is presented using Matlab-Simulink and X-Plane.

This paper has the following structure. Section 2 introduces the aircraft's lateral-directional dynamics. Section 3 is devoted to designing the guidance and control algorithms, while Section 4 reports the numerical simulation results. The paper ends in Section 5 with concluding remarks.

2 Aircraft lateral-directional dynamics

Under the assumption that there is a controller for the aircraft longitudinal dynamics that holds the flight path angle γ and the aircraft aerodynamic speed V at some constant values $\bar{\gamma}$ and $\bar{V}$, respectively, the aircraft lateral-directional dynamics reads as [14][1]

$$\begin{aligned} m\bar{V}\dot{\beta} &= mg(c_\beta s_\phi c_{\bar{\theta}} + s_\beta c_{\bar{\alpha}} s_{\bar{\theta}} - s_{\bar{\alpha}} s_\beta c_{\bar{\theta}} c_\phi) \\ &\quad + m\bar{V}(p s_{\bar{\alpha}} - r c_{\bar{\alpha}}) \\ &\quad + \bar{T} s_\beta c_{\bar{\alpha}} + \bar{q} S C_Y(\beta, p, r, \delta_r) \end{aligned} \tag{1}$$

$$\begin{aligned} \begin{bmatrix} I_x\dot{p} - I_{xz}\dot{r} \\ I_z\dot{r} - I_{xz}\dot{p} \end{bmatrix} &= \begin{bmatrix} -(I_z - I_y)r^2 t_\phi + I_{xz} p r t_\phi \\ -(I_y - I_x) p r t_\phi - I_{xz} r^2 t_\phi \end{bmatrix} \\ &\quad + \bar{q} S b \begin{bmatrix} c_l(\beta, p, r, \delta_a, \delta_r) \\ c_n(\beta, p, r, \delta_a, \delta_r) \end{bmatrix} \end{aligned} \tag{2}$$

where m is the aircraft mass, β, ϕ, $\bar{\theta}$, $\bar{\alpha}$ are the sideslip, roll, pitch and attack angles, respectively. Moreover, p and r are the roll and yaw angular speeds expressed in body axes, $\bar{T}$ is the power plant thrust, I_x, I_y, I_z and I_{xz} are the aircraft inertia moments, b is the wingspan, S is the aircraft wing surface, and $\bar{q} = 1/2\rho\bar{V}^2$ with ρ the air density. Finally, C_Y, c_l and c_n are the aerodynamic coefficientes of the lateral force and the roll and yaw moments with δ_a and δ_r the ailerons and rudder deflections. In equation (1), $\bar{\theta}$ and $\bar{\alpha}$ are the constant values that agree with $\bar{\gamma} = \bar{\theta} - \bar{\alpha}$.

[1] In the rest of the paper, the notation $\cos(\sigma_1 + \sigma_2) = c_{\sigma_1+\sigma_2}$, $\sin(\sigma_1 + \sigma_2) = s_{\sigma_1+\sigma_2}$ and $\tan(\sigma_1) = t_{\sigma_1}$ for any angles σ_1, σ_2 is considered.

The following equations describe the aircraft lateral-directional kinematic [15]

$$\begin{bmatrix} \dot{x} \\ \dot{y} \\ \dot{\phi} \\ \dot{\psi} \end{bmatrix} = \begin{bmatrix} c_1\bar{V} \\ c_2\bar{V} \\ p + t_{\bar{\theta}}\frac{r}{c_\phi} \\ \frac{1}{c_{\bar{\theta}}}\frac{r}{c_\phi} \end{bmatrix} \tag{3}$$

where x and y represent the aircraft Cartesian position, $\chi = \psi - \beta$ is the azimuth angle, and

$$\begin{aligned} c_1 &= -c_{\chi+\beta} s_{\bar{\alpha}+\bar{\gamma}} s_\beta s_\phi c_{\bar{\alpha}} - s_{\chi+\beta} s_\beta c_\phi c_{\bar{\alpha}} \\ &\quad + c_{\bar{\alpha}+\bar{\gamma}} c_{\chi+\beta} c_\beta c_{\bar{\alpha}} + c_{\chi+\beta} s_{\bar{\alpha}+\bar{\gamma}} c_\phi s_{\bar{\alpha}} \\ &\quad - s_{\chi+\beta} s_\phi s_{\bar{\alpha}} \\ c_2 &= -s_{\chi+\beta} s_{\bar{\alpha}+\bar{\gamma}} s_\beta s_\phi c_{\bar{\alpha}} + s_{\chi+\beta} c_{\bar{\alpha}+\bar{\gamma}} c_\beta c_{\bar{\alpha}} \\ &\quad + s_{\chi+\beta} s_{\bar{\alpha}+\bar{\gamma}} c_\phi s_{\bar{\alpha}} + c_{\chi+\beta} s_\beta c_\phi c_{\bar{\alpha}} \\ &\quad + c_{\chi+\beta} s_\phi s_{\bar{\alpha}}) \end{aligned}$$

The lateral control design considers the following assumption on the lateral-directional kinematic and dynamic models.

Assumption 1 The aerodynamic angles are small, this is,

$$\bar{\alpha} \approx 0 \;\rightarrow\; \bar{\gamma} = \bar{\theta}, \quad \beta \approx 0 \;\rightarrow\; \chi = \psi \tag{4}$$

and the lateral force is equal zero, this is,

$$C_Y = 0 \tag{5}$$

The assumption expressed in equation (4) has also been considered in reference [10]. On the other hand, equations (4) and (5) imply that the coordinated turn condition [16]

$$\frac{g}{\bar{V}} s_\phi c_{\bar{\theta}} - r = 0 \tag{6}$$

holds. Finally, the lateral-directional model considered in this work is described by the equation (2) and

$$\begin{bmatrix} \dot{x} \\ \dot{y} \\ \dot{\phi} \\ \dot{\psi} \end{bmatrix} = \begin{bmatrix} c_{\bar{\gamma}} c_\chi \bar{V} \\ c_{\bar{\gamma}} s_\chi \bar{V} \\ p + t_{\bar{\theta}}\frac{r}{c_\phi} \\ \frac{1}{c_{\bar{\theta}}}\frac{r}{c_\phi} \end{bmatrix} \tag{7}$$

3 Lateral guidance control

This section presents the control design procedure. First, the control objective is defined as follows.

Control objective Design control inputs δ_a and δ_r such that the lateral aircraft position error $\tilde{y} = y - y_d$ with y_d a constant reference converges to zero, see Figure 1. This work follows the inner-outer control-loop approach to designing the lateral guidance algorithm. The control objective for the inner-loop controller is expressed as follows

$$\lim_{t\to T} \tilde{p} \to 0, \quad \lim_{t\to T} \tilde{r} \to 0 \tag{8}$$

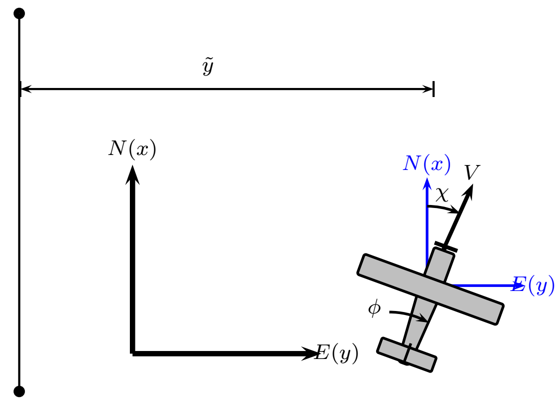

Figure 1: Lateral aircraft error distance $\tilde{y}$.

with T a bounded positive time. Moreover, $\tilde{r} = r - r_d$ and $\tilde{p} = p - p_d$, with p_d and r_d the angular speeds references determined by the outer-loop controller.

A controller with finite-time convergence can be designed as follows. Consider that the aerodynamic moment coefficients have the following structure [15]

$$
\begin{aligned}
c_l &= c_{l_0} + c_{l_\beta}\beta + \frac{b}{2\bar{V}}c_{l_p}p + \frac{b}{2\bar{V}}c_{l_r}r \\
&\quad + c_{l_{\delta_a}}\delta_a + c_{l_{\delta_r}}\delta_r \\
c_n &= c_{n_0} + c_{n_\beta}\beta + \frac{b}{2\bar{V}}c_{n_p}p + \frac{b}{2\bar{V}}c_{n_r}r \\
&\quad + c_{n_{\delta_a}}\delta_a + c_{n_{\delta_r}}\delta_r
\end{aligned}
$$

with c_{i_0}, c_{i_β}, c_{i_p} and c_{i_r} with $i = l, n$ the aerodynamic stability coefficients and $c_{i_{\delta_a}}$, $c_{i_{\delta_r}}$ with $i = l, n$ the aerodynamic control coefficients, the rotational dynamics can be expressed as

$$
\begin{bmatrix} \dot{p} \\ \dot{r} \end{bmatrix} = \begin{bmatrix} \varphi_1(\beta,p,r) \\ \varphi_2(\beta,p,r) \end{bmatrix} + B \begin{bmatrix} \delta_a \\ \delta_r \end{bmatrix} \tag{9}
$$

with

$$
B = \bar{q}Sb \begin{bmatrix} I_x & -I_{xz} \\ -I_{xz} & I_z \end{bmatrix}^{-1} \begin{bmatrix} c_{l_{\delta_a}} & c_{l_{\delta_r}} \\ c_{n_{\delta_a}} & c_{n_{\delta_r}} \end{bmatrix}
$$

Define

$$
\mathbf{S} = \begin{bmatrix} \tilde{p} \\ \tilde{r} \end{bmatrix}
$$

then

$$
\dot{\mathbf{S}} = \begin{bmatrix} \varphi_1(\beta,p,r) \\ \varphi_2(\beta,p,r) \end{bmatrix} + B \begin{bmatrix} \delta_a \\ \delta_r \end{bmatrix} - \begin{bmatrix} \dot{p}_d \\ \dot{r}_d \end{bmatrix}
$$

The super twisting algorithm proposes the next control input [17][2]

$$
B \begin{bmatrix} \delta_a \\ \delta_r \end{bmatrix} = -\Lambda_2 \int_0^t \mathbf{sign}(\mathbf{S}(\tau))d\tau - \Lambda_1 \,\mathbf{abs}(\mathbf{S})^{\frac{1}{2}}\,\mathbf{sign}(\mathbf{S}) \tag{10}
$$

where

$$
\Lambda_1 = \mathrm{diag}\{\lambda_{11}, \lambda_{12}\}, \; \Lambda_2 = \mathrm{diag}\{\lambda_{21}, \lambda_{22}\}
$$

with $\lambda_{i1}, \lambda_{i2}$, $i = 1, 2$ positive gains. Thus, one gets

$$
\begin{aligned}
\dot{\mathbf{S}} &= \begin{bmatrix} \varphi_1(\beta,p,r) \\ \varphi_2(\beta,p,r) \end{bmatrix} - \begin{bmatrix} \dot{p}_d \\ \dot{r}_d \end{bmatrix} \\
&\quad -\Lambda_2 \int_0^t \mathbf{sign}(\mathbf{S}(\tau))d\tau - \Lambda_1 \,\mathbf{abs}(\mathbf{S})^{\frac{1}{2}}\,\mathbf{sign}(\mathbf{S})
\end{aligned}
$$

the bold functions absolute and sign are vector functions evaluated element-wise.

Consider the following change of coordinates

$$
\begin{aligned}
\mathbf{S}_1 &= \mathbf{S} \\
\mathbf{S}_2 &= \Theta(\beta,p,r,t) - \Lambda_2 \int_0^t \mathbf{sign}(\mathbf{S}(\tau))d\tau
\end{aligned}
$$

where

$$
\Theta(\beta,p,r,t) = \begin{bmatrix} \varphi_1(\beta,p,r) \\ \varphi_2(\beta,p,r) \end{bmatrix} - \begin{bmatrix} \dot{p}_d \\ \dot{r}_d \end{bmatrix}
$$

Then, it follows that

$$
\begin{aligned}
\dot{\mathbf{S}}_1 &= -\Lambda_1 \,\mathbf{abs}(\mathbf{S}_1)^{\frac{1}{2}}\,\mathbf{sign}(\mathbf{S}_1) + \mathbf{S}_2 \\
\dot{\mathbf{S}}_2 &= -\Lambda_2 \,\mathbf{sign}(\mathbf{S}_1) + \dot{\Theta}
\end{aligned} \tag{11}
$$

Proposition 1 Assume that matrix B is known, and

$$
|\dot{\Theta}| \leq \Theta_0 \tag{12}
$$

for some positive bounded Θ_0. Then, there exist positive definite matrices Λ_1 and Λ_2 such that the closed-loop dynamics (9) and (10) satisfy (8).

Proof. Equation (11) can be expanded as follows

$$
\begin{aligned}
\dot{s}_{11} &= -\lambda_{11}|s_{11}|^{\frac{1}{2}}\,\mathrm{sign}(s_{11}) + s_{21} \\
\dot{s}_{21} &= -\lambda_{21}\,\mathrm{sign}(s_{11}) + \dot{\Theta}_1 \\
\dot{s}_{12} &= -\lambda_{12}|s_{12}|^{\frac{1}{2}}\,\mathrm{sign}(s_{12}) + s_{22} \\
\dot{s}_{22} &= -\lambda_{22}\,\mathrm{sign}(s_{11}) + \dot{\Theta}_2
\end{aligned}
$$

where the following notation is considered $S_1 = \begin{bmatrix} s_{11} & s_{12} \end{bmatrix}^\top$, $S_2 = \begin{bmatrix} s_{21} & s_{22} \end{bmatrix}^\top$ and $\Theta =$

[2] This is, for any vector $\chi \in \mathbb{R}^2$

$$
\mathbf{sign}(\chi) = \begin{bmatrix} \mathrm{sign}(\chi_{11}) \\ \mathrm{sign}(\chi_{12}) \end{bmatrix}, \; \mathbf{abs}(\chi)^{\frac{1}{2}}\,\mathbf{sign}(\chi) = \begin{bmatrix} |\chi_{11}|^{\frac{1}{2}}\,\mathrm{sign}(\chi_{11}) \\ |\chi_{12}|^{\frac{1}{2}}\,\mathrm{sign}(\chi_{12}) \end{bmatrix}
$$

$\begin{bmatrix} \Theta_1 & \Theta_2 \end{bmatrix}^\top$. Thus, (s_{11}, s_{21}) and (s_{12}, s_{22}) define two super-twisting algorithms [17]. As shown in [18], if (12) holds, the states (s_{11}, s_{21}),$(s_{12}, \text{and} s_{22})$ converge to zero in finite-time so that S_1 and S_2 converge to zero in finite time. ◁

Now the control design procedure focus on the kinematic model (7). Expresing (7) in terms of $\tilde{p}$ and $\tilde{r}$ gives

$$\begin{bmatrix} \dot{x} \\ \dot{y} \\ \dot{\phi} \\ \dot{\psi} \end{bmatrix} = \begin{bmatrix} c_{\bar{\theta}} c_\psi \bar{V} \\ c_{\bar{\theta}} s_\psi \bar{V} \\ p_d + t_{\bar{\theta}} \frac{r_d}{c_\phi} \\ \frac{1}{c_{\bar{\theta}}} \frac{r_d}{c_\phi} \end{bmatrix} + \begin{bmatrix} 0 \\ 0 \\ \tilde{p} + t_{\bar{\theta}} \frac{\tilde{r}}{c_\phi} \\ \frac{1}{c_{\bar{\theta}}} \frac{\tilde{r}}{c_\phi} \end{bmatrix} \quad (13)$$

where the assumption expressed in equation (4) is considered. Assume that $t > T$, and select

$$r_d = \frac{g}{\bar{V}} c_{\bar{\theta}} s_\phi \quad (14)$$

to achieve the coordinated turn condition. As a result, equation (13) becomes

$$\begin{bmatrix} \dot{x} \\ \dot{y} \\ \dot{\phi} \\ \dot{\psi} \end{bmatrix} = \begin{bmatrix} c_{\bar{\theta}} c_\psi \bar{V} \\ c_{\bar{\theta}} s_\psi \bar{V} \\ p_d + \frac{g}{\bar{V}} s_{\bar{\theta}} t_\phi \\ \frac{g}{\bar{V}} t_\phi \end{bmatrix} \quad (15)$$

In equation (15) the only control input is p_d; thus, defining a reference for the roll angle, ϕ the yaw angle ψ can be modified so that the lateral aircraft position y can be driven to the desired value y_d; this is the guidance problem considered in [12]. If the airspeed $\bar{V}$ is not constant, the aircraft translational kinematic is equal to the translational kinematic of the unicycle mobile robot as studied in [13] with the only difference that the speed $\bar{V}$ cannot take negative values in the aircraft case.

As expressed in equation (15), it looks that the configuration space for the yaw angle ψ is $\mathbb{R}$; however, this is not the case; its configuration space is $\mathbb{S}^1$ [3], the unit circle. The unit circle can be projected to the Lie group $SO(2)$ as [19][4]

$$\forall \psi \in [0, 2\pi] \quad \exists \quad R_\psi \in SO(2)$$

where

$$SO(2) = \left\{ R_\psi \in \mathbb{R}^{2\times 2} | R_\psi^\top R_\psi = I, \det(R_\psi) = 1 \right\}$$

with $I \in \mathbb{R}^{2\times 2}$ the identity matrix. In local coordinates, one has

$$R_\psi = \begin{bmatrix} c_\psi & -s_\psi \\ s_\psi & c_\psi \end{bmatrix} \quad (16)$$

[3]
$$\mathbb{S}^1 = \left\{ P \in \mathbb{R}^2 | P^\top P = 1 \right\}$$

[4]The roll angle ϕ has also a configuration space equal to $\mathbb{S}^1$ but in this work this fact is not considered.

The aircraft kinematic in (15) in terms of the matrix (16) can be expressed as

$$\begin{array}{rcl} \begin{bmatrix} \dot{x} \\ \dot{y} \end{bmatrix} & = & \begin{bmatrix} c_\psi & -s_\psi \\ s_\psi & c_\psi \end{bmatrix} \begin{bmatrix} V c_{\bar{\theta}} \\ 0 \end{bmatrix} \\ \frac{d}{dt}\left(\begin{bmatrix} c_\psi & -s_\psi \\ s_\psi & c_\psi \end{bmatrix} \right) & = & \begin{bmatrix} c_\psi & -s_\psi \\ s_\psi & c_\psi \end{bmatrix} \begin{bmatrix} 0 & -\frac{g}{V} t_\phi \\ \frac{g}{V} t_\phi & 0 \end{bmatrix} \\ \dot{\phi} & = & \frac{g}{V} s_{\bar{\theta}} t_\phi + p_d \end{array}$$

in compact form

$$\begin{array}{rcl} \dot{X} & = & R_\psi \mathcal{V} \\ \dot{R}_\psi & = & R_\psi \bar{r}^\wedge \\ \dot{\phi} & = & \bar{r} s_{\bar{\theta}} + p_d \end{array} \quad (17)$$

with

$$X = \begin{bmatrix} x \\ y \end{bmatrix}, \; \mathcal{V} = \begin{bmatrix} \bar{v} \\ 0 \end{bmatrix}, \; \bar{r}^\wedge = \begin{bmatrix} 0 & -\bar{r} \\ \bar{r} & 0 \end{bmatrix}$$

Moreover,

$$\bar{v} = \bar{V} c_{\bar{\theta}}, \quad \bar{r} = \frac{g}{V} t_\phi \quad (18)$$

and the map $(\cdot)^\wedge : \mathbb{R} \to \mathfrak{so}(2)$ that projects the angular speed $\bar{r}$ to the Lie algebra $\mathfrak{so}(2)$ of $SO(2)$ is characterized as [20]

$$\mathfrak{so}(2) = \left\{ \begin{bmatrix} 0 & -\bar{r} \\ \bar{r} & 0 \end{bmatrix}, \forall \, \bar{r} \in \mathbb{R} \right\}$$

Hence, $R_\psi \bar{r}^\wedge$ is the tangent space of $SO(2)$ at R_ψ with angular speed $\bar{r}$.

From equation (17) it is clear that the lateral guidance error $\tilde{y}$ can be only commanded though the matrix R_ψ. Hence, the error between R_ψ and R_{ψ_d} is defined as

$$\tilde{R}_\psi = R_{\psi_d}^\top R_\psi \quad (19)$$

with R_{ψ_d} the desired rotation matrix.

Then, it follows that

$$\dot{X} = R_{\psi_d} \tilde{R}_\psi \mathcal{V}$$

Now, the control objective is to command $\tilde{R}_\psi$ to the identity matrix I in such a way that the translational kinematics asymptotically becomes

$$\dot{X} = R_{\psi_d} \mathcal{V} \quad (20)$$

To define the desired rotation matrix R_{ψ_d} consider that equation (20) can be expressed as

$$\begin{array}{rcl} \dot{x} & = & \bar{v} c_{\psi_d} \\ \dot{y} & = & \bar{v} s_{\psi_d} \end{array} \quad (21)$$

In equation (21) the virtual control input is s_{ψ_d} therefore it must be a signal that takes values in the set $[-1, 1]$.

The following virtual control input is selected, to satisfy that $s_{\psi_d} \in [-1, 1]$,

$$s_{\psi_d} = -\tanh(k\tilde{y})$$

with k a positive constant. Hence, the desired rotation matrix becomes

$$R_{\psi_d} = \begin{bmatrix} \sqrt{1-\tanh(k\tilde{y})^2} & \tanh(k\tilde{y}) \\ -\tanh(k\tilde{y}) & \sqrt{1-\tanh(k\tilde{y})^2)} \end{bmatrix}$$

Remark 1 It is easy to verify that R_{ψ_d} belongs to $SO(2)$; as a consequence, the matrix error definition in equation (19) ensures that $\tilde{R}_\psi$ also belongs to $SO(2)$.

The rotation matrix error dynamics is described by

$$\dot{\tilde{R}}_\psi = \tilde{R}_\psi \tilde{\bar{r}}^\wedge \tag{22}$$

where

$$\tilde{\bar{r}} = \bar{r} - \bar{r}_d, \quad \bar{r}_d = (R_{\psi_d}^\top \dot{R}_{\psi_d})^\vee$$

with

$$\dot{R}_{\psi_d} = k\bar{v}s_\psi \begin{bmatrix} -r_{11} & 1-\tanh(k\tilde{y})^2 \\ 1-\tanh(k\tilde{y})^2 & -r_{11} \end{bmatrix}$$

$$r_{11} = \sqrt{1-\tanh(k\tilde{y})^2}\tanh(k\tilde{y}),$$

and the map $(\cdot)^\vee : \mathfrak{so}(2) \to \mathbb{R}$ is the inverse map of $(\cdot)^\wedge$ defined as [20]

$$(\bar{r}^\wedge)^\vee = \left(\begin{bmatrix} 0 & -\bar{r} \\ \bar{r} & 0 \end{bmatrix} \right)^\vee = \bar{r},\ \forall \bar{r}^\wedge \in \mathfrak{so}(2),\ \bar{r} \in \mathbb{R}$$

Finally,

$$\bar{r} = (R_{\psi_d}^\top \dot{R}_{\psi_d})^\vee - k_R P_a(\tilde{R}_\psi)^\vee \tag{23}$$

with $P_a(\tilde{R}_\psi) = \frac{1}{2}(\tilde{R}_\psi - \tilde{R}_\psi^\top)$ and k_R a positive gain. Thus, one has

Proposition 2 Consider the matrix error dynamics in equation (22) in closed-loop with the control law (23). Then, there exist a gain k_R such that the equilibrium point $\tilde{R}_\psi = I$ is almost globally asymptotically stable.[5]

Proof. The closed-loop dynamics (22)-(23) reads as

$$\dot{\tilde{R}}_\psi = -k_R \tilde{R} P_a(\tilde{R}_\psi) \tag{24}$$

The equilibrium points are characterized by the following matrix algebraic equation

$$0 = -k_R \tilde{R}_\psi P_a(\tilde{R}_\psi)$$

It can be proven that the solutions to the above equation are $\tilde{R}_\psi \pm I$. Linearizing the closed-loop dynamic (24) around both equilibrium points it can be verified that the equilibrium point $\tilde{R}_\psi = -I$ is unstable. Consider now the following Lyapunov function [23]

$$\Phi = \frac{1}{2}\,\mathrm{trace}(I - \tilde{R}_\psi)$$

The time derivative of Φ is

$$\dot{\Phi} = -k_R \left(P_a(\tilde{R}_\psi)^\vee \right)^2$$

thus, the closed-loop trajectories converge to the set [24]

$$\mathcal{D} = \left\{ \tilde{R}_\psi \in SO(2) \,|\, P_a(\tilde{R}_\psi) = 0 \right\}$$

that only contains the matrices $\tilde{R}_\psi = \pm I$, thus, the proof is completed. ◁

Now, defining, from equation (18)

$$\zeta = \frac{g}{\bar{V}} t_\phi - \bar{r}$$

it follows that

$$\dot{\zeta} = \frac{g}{\bar{V}}(1+t_\phi^2)\left(p_d + \frac{g}{\bar{V}} s_{\bar{\theta}} t_\phi \right) - \dot{\bar{r}} \tag{25}$$

thus, one has

Proposition 3 Assume that $\phi \in (-\pi/2, \pi/2)$. Then, the dynamic system in (25) in closed-loop with the control law

$$p_d = -\frac{g}{\bar{V}} s_{\bar{\theta}} t_\phi + \frac{\bar{V}}{g(1+t_\phi^2)}(-K\zeta + \dot{\bar{r}}) \tag{26}$$

where K is a positive constant has a locally exponentially stable equilibrium point at $\zeta = 0$.

Proof. The closed-loop dynamics (25)-(26) is described by

$$\dot{\zeta} = -K\zeta$$

thus, ζ converges exponentially to zero if the constraint $\phi \in (-\pi/2, \pi/2)$ holds. ◁

Remark 2 This last result shows a disadvantage that arises by not considering the configuration space of the states. Even though there is no physical reason to constraint ϕ to the set (A), it must be constrained due to the use of local coordinates.

The main results reads as follows

Proposition 4 Consider the lateral-directional dynamics (7)-(2) in closed-loop with the controller (10)-(26) and the guidance algorithm (23). Then, there exists gains Λ_1, Λ_2, k, k_R and K such that the error distance $\tilde{y}$ locally asymptotically converges to zero.

[5] An equilibrium solution of a dynamical system is said to be almost globally asymptotically stable if it is asymptotically stable with an almost global domain of attraction, i.e., the domain of attraction is the entire state space excluding a set of Lebesgue measure zero [21], [22].

Proof. From propositions 1, 2, 3, and 4, no signals can escape to infinity in a finite time. Hence, to achieve that $\tilde{y}$ converges asymptotically to zero, the control gains need to be selected in such a way that the errors $\tilde{r}$ and $\tilde{p}$ converge to zero faster than ζ and $\tilde{R}_\psi$ converging to I. The gains k_R, K need to be selected in such a way that ζ converges to zero faster than $\tilde{R}_\psi$ converges to I. The control authority to drive $\tilde{y}$ to zero is the aircraft yaw angle which cannot take significant values. Thus, the slower gain must be k.

If the errors $\tilde{r}$, $\tilde{p}$, ζ and $\tilde{R}_\psi$ converge to their references, from equation (20), one has

$$\begin{aligned} \dot{x} &= \bar{v}\sqrt{1-\tanh(k\tilde{y}^2)} \\ \dot{y} &= -\bar{v}\tanh(k\tilde{y}) \end{aligned} \tag{27}$$

From the second equation in (27) it can be shown that $\tilde{y}$ converges to zero. As it can be observed in (27) the speed $\dot{x}$ remain bounded and the speed $\bar{v}$ improves the convergence performance. ◁

4 Numerical simulations

In this section, the numerical simulation results are reported. The control and guidance algorithms are computed in Simulink while the X-Plane flight simulator runs the aircraft dynamic model. The communication between Simulink and X-Plane uses the User Datagram Protocol (UDP) [25].

The remote-controlled aircraft known as Telemaster was modeled in Plane Maker, a program bundled with X-Plane that allows design aircraft, see Figure 2. The aircraft's main parameters are $I_x = 11.671\text{kgm}^2$, $I_z = 17.285\text{kgm}^2$, $I_{xz} = -0.024\text{kgm}^2$, $b = 2.386\text{m}$, and $S = 0.858\text{m}^2$. The aerodynamic control coefficients $c_{n_{\delta_a}} = 0.4762$, $c_{n_{\delta_r}} = 1.5888$, $c_{l_{\delta_a}} = 0.8507$, $c_{n_{\delta_a}} = 0.0.0154$ were obtained using the SIDPAC software introduced in [15].

Figure 2: Telemaster modeled in Plane Maker.

A modified version of the longitudinal dynamic controller introduced in [26] is implemented. The aircraft aerodynamic speed and the flight path angle are regulated at $\bar{V} = 20\text{m/s}$, and $\bar{\gamma} = 1\text{deg}$.

The control gain tunning required some experimental tests. After these test it is concluded that the gain Λ_1 modifies the oscillations after p and r have reached p_d and r_d, respectively. The gain Λ_2 adjusts the time it takes to p and r to reach the desired reference. Small values for Λ_1 and λ_2 produce a slow response and large amplitude oscillations in steady-state. On the contrary, significant values for gains λ_1 and Λ_2 produce a fast response and high-frequency, low amplitude oscillations, which in some cases lead to instability.

The gains K and k_R also required several tests; the tunning criteria avoided extensive paths for the roll angle. Finally, the gain k was lowered little by little to reach a reference change of 100m without saturating the aileron and rudder deflection. Large k values demand a more considerable effort to the lateral controller producing large deflections for control surfaces. Small k values allow significant reference changes, but the lateral convergence error will be slow.In conclusion, the gain k must be tuned according to the required mission characteristics. The tunned controller gains are Λ_1 =diag$\{2,3\}$, Λ_2 =diag$\{5,8\}$, $K = 1.5$, $k_R = 1.25$, and $k = 0.004$.

The aircraft takes off from the Atizapan de Zaragoza local airport (MMJC) near Mexico City. The reported air density was 0.9629kg/m^3. During the first 45s, only the longitudinal controller and a PD yaw controller are working. The PD yaw controller tries to keep the aircraft along the runway. The plane has enough altitude at the second 47 to activate the proposed controller and lateral guidance algorithm.

Figure 3 shows the lateral error behavior. The proposed control and guidance algorithm enters into action at 47s with $y(47) = 22200\text{m}$ and $y_d = 22300\text{m}$. As it can be observed, the lateral error converges to zero, the transients at 130s and 210s are due to the reference change, $y_d = 22400\text{m}$ and $y_d = 22300\text{m}$, respectively. The aircraft reaches the first reference; then it moves 100m to the right; after the error converges to zero, it returns to its first reference, 100m to the left. It is important to mention that the jump at second 52, approximately, is due to the fact that the algorithm tries to orientate the aircraft in the direction of the line before it tries to reduce the lateral error. Figure 4 depicts the attitude error which in $SO(2)$ is measured by the term $(P_a(\tilde{R}_\psi))^\vee$. As it can be observed, this attitude error converges to zero after the transient due to lateral position reference changes. Note that the attitude error is dimensionless. However, the gain k_R can be used to obtain the same dimension as $\bar{r}$,$(1/s)$. Figure 5 shows the time history of roll angle. It can be observed that a roll maneuver is not required unless there is a reference change. Figure 6 presents the roll and yaw rate error $\tilde{p}$ and $\tilde{r}$. The proposed controller tries to keep the roll and yaw rate error in zero. Even if it seems

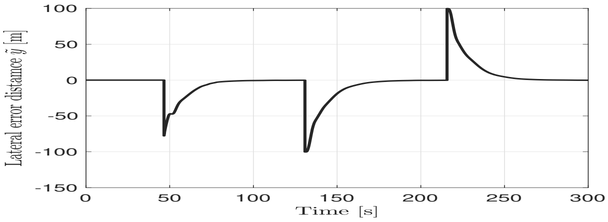

Figure 3: Lateral distance error $\tilde{y}$.

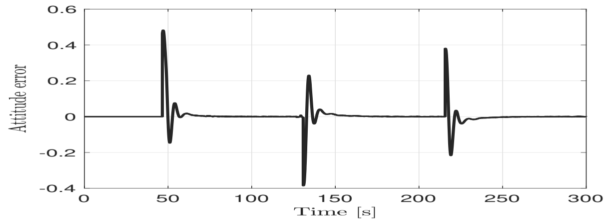

Figure 4: Attitude error $(P_a(\tilde{R}_\psi))^\vee$.

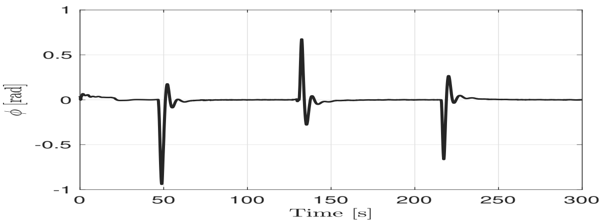

Figure 5: Roll angle.

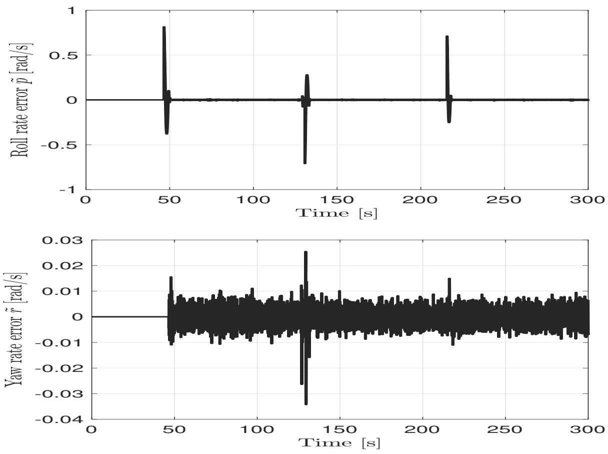

Figure 6: Rotational speed errors p_d (above), r_d (down).

that the yaw rate error is oscillating, these oscillations have a low amplitude, showing that the lateral guidance algorithm is giving good results. Figure 7 shows the control inputs, the aileron, and rudder deflections. Note that the required control surface's deflection remains bounded. Finally, figure 8 presents the coordinated turn condition. As it can be observed, the condition is accomplished with some low amplitude oscillations, except when there is a reference change. The link https://www.youtube.com/watch?v=LXomSgZlFt0 shows the X-Plane simulation.

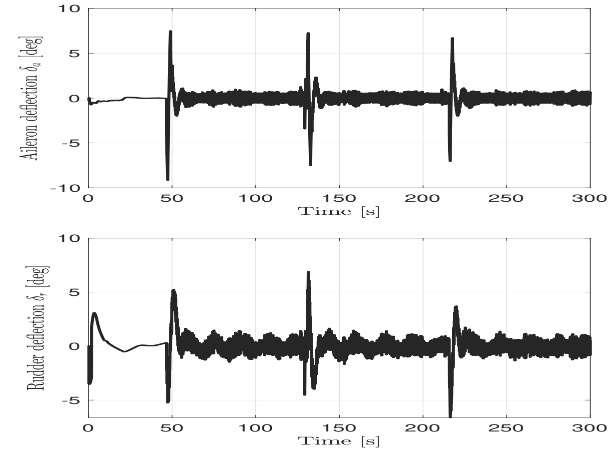

Figure 7: Aileron deflection δ_a (above), rudder deflection δ_r (down).

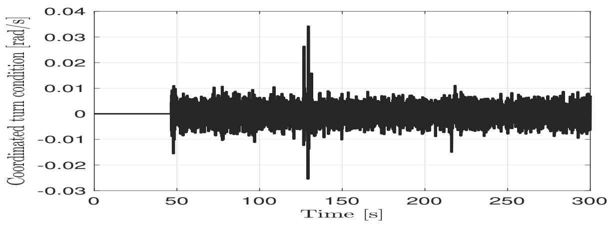

Figure 8: Attitude error $(P_a(\tilde{R}_\psi))^\vee$.

5 Conclusions

A nonlinear controller and a guidance algorithm for the lateral-directional aircraft dynamics were proposed. The nonlinear controller is based on the second-order sliding mode controller, the super twisting algorithm, which guarantees finite-time convergence. The guidance algorithm is designed taking into account the geometric properties of the configuration space of the yaw angle. Numerical simulations showed that the proposed guidance algorithm drives the aircraft lateral error distance to zero. The whole controller and guidance algorithms are implemented in Matlab-Simulink and X-Plane flight simulator.

Acknowledgements

The fitst author thanks CONACYT for the economic support with the scholarships CVU ID: 1079221.

References

[1] Ying Luo, Haiyang Chao, Long Di, and YangQuan Chen. Lateral directional fractional order (pi) α control of a small fixed-wing unmanned aerial vehicles: controller designs and flight tests. IET control theory & applications, 5(18):2156–2167, 2011.

[2] R Samar, Shakil Ahmed, and Faisal Aftab. Lateral control with improved performance for uavs. IFAC Proceedings Volumes, 40(7):37–42, 2007.

[3] Sanghyuk Park, John Deyst, and Jonathan How. A new nonlinear guidance logic for trajectory tracking. In AIAA guidance, navigation, and control conference and exhibit, pages 1–16, 2004.

[4] Mehdi Golestani and Iman Mohammadzaman. Pid guidance law design using short time stability approach. Aerospace Science and Technology, 43:71–76, 2015.

[5] Takeshi Yamasaki, SN Balakrishnan, and Hiroyuki Takano. Integrated guidance and autopilot design for a chasing uav via high-order sliding modes. Journal of the Franklin Institute, 349(2):531–558, 2012.

[6] Syed Ussama Ali, Raza Samar, M. Zamurad Shah, Aamer I. Bhatti, Khalid Munawar, and Ubaid M. Al-Sggaf. Lateral guidance and control of uavs using second-order sliding modes. Aerospace Science and Technology, 49:88–100, 2016.

[7] P Zarchan. Tactical and strategic missile guidance fourth edition. PROGRESS IN ASTRONAUTICS AND AERONAUTICS, 199, 2002.

[8] Pini Gurfil, Mario Jodorkovsky, and Moshe Guelman. Finite time stability approach to proportional navigation systems analysis. Journal of Guidance, Control, and Dynamics, 21(6):853–861, 1998.

[9] Iman Mohammad Zaman and Hamid Reza Momeni. Pi guidance law design using circle criterio. Journal of Control, 4(2):11–19, 2010.

[10] Johannes Stephan, Ole Pfeifle, Stefan Notter, Federico Pinchetti, and Walter Fichter. Precise tracking of extended three-dimensional dubins paths for fixed-wing aircraft. Journal of Guidance, Control, and Dynamics, 43(12):2399–2405, 2020.

[11] Rolf Rysdyk. Unmanned aerial vehicle path following for target observation in wind. Journal of Guidance, Control, and Dynamics, 29(5):1092–1100, 2006.

[12] Marius Niculescu. Lateral track control law for aerosonde uav. In 39th Aerospace Sciences Meeting and Exhibit, pages 1–11, 2001.

[13] Wei Ren and Randy W Beard. Trajectory tracking for unmanned air vehicles with velocity and heading rate constraints. IEEE Transactions on Control Systems Technology, 12(5):706–716, 2004.

[14] José J Corona-Sánchez, Óscar Roberto Guzmán Caso, and H Rodríguez-Cortés. A coordinated turn controller for a fixed-wing aircraft. Proceedings of the Institution of Mechanical Engineers, Part G: Journal of Aerospace Engineering, 233(5):1728–1740, 2019.

[15] Eugene A Morelli and Vladislav Klein. Aircraft system identification: theory and practice, volume 2. Sunflyte Enterprises Williamsburg, VA, 2016.

[16] Brian L Stevens, Frank L Lewis, and Eric N Johnson. Aircraft control and simulation: dynamics, controls design, and autonomous systems. John Wiley & Sons, 2015.

[17] A. Chalanga, S. Kamal, L. M. Fridman, B. Bandyopadhyay, and J. A. Moreno. Implementation of super-twisting control: Super-twisting and higher order sliding-mode observer-based approaches. IEEE Transactions on Industrial Electronics, 63(6):3677–3685, 2016.

[18] Jaime A. Moreno and Marisol Osorio. Strict lyapunov functions for the super-twisting algorithm. IEEE Transactions on Automatic Control, 57(4):1035–1040, 2012.

[19] J. E. Marsden and T. S. Ratiu. Introduction to Mechanics and Symmetry: A Basic Exposition of Classical Mechanical Systems. Texts in applied mathematics. Springer, 1999.

[20] Marián Fecko. Differential Geometry and Lie Groups for Physicists. Cambridge University Press, 2006.

[21] Taeyoung Lee. Global exponential attitude tracking controls on $\mathsf{so}(3)$. IEEE Transactions on Automatic Control, 60(10):2837–2842, 2015.

[22] E. M. Coates and T. I. Fossen. Geometric reduced-attitude control of fixed-wing uavs. Applied Sciences, 11(7), 2021.

[23] Daniel E. Koditschek. The application of total energy as a Lyapunov function for mechanical control systems. Contemporary Mathematics, 97:131, 1989.

[24] H. K. Khalil. Nonlinear Systems. Pearson Education. Prentice Hall, 2002.

[25] Peter Thomas. X-Plane Blockset. MATLAB Central File Exchange, Retrieved February 25, 2022.

[26] I. Rosario-Gabriel and H. Rodríguez Cortés. Aircraft longitudinal control based on the lanchester's phugoid dynamics model. In 2018 International Conference on Unmanned Aircraft Systems (ICUAS), pages 924–929, 2018.